Submitted: 01/14/19

Research Article

Jed Lenetsky[1], Bruno Tremblay[2], Charles Brunette[2]

[1]McGill School of Environment, McGill University
[2]Department of Atmospheric and Oceanic Science, McGill University

Variability and Predictability of the Bering Strait Ocean Heat Transport and Arctic Ocean Sea Ice Extent

Keywords

Sea ice extent, Bering Strait, Ocean Heat transport, Forecasting, Arctic

Email Correspondence

jed.lenetsky@mail.mcgill.ca

Abstract

Background: This study examines the monthly, seasonal, and interannual variations in Pacific Ocean heat transport entering the Arctic Ocean through the Bering Strait, and its influence on sea ice extent in the Arctic Ocean.

Methods: Monthly ocean heat transport is calculated using temperature and volumetric transport data from moorings deployed in the Bering Strait. Pearson correlations are calculated between the observed detrended monthly cumulative Bering Strait ocean heat transport and the detrended monthly sea ice extent time series from May through September.

Results: An increase in the spring variability of the Bering Strait ocean heat transport is found since 2010, associated with both increased volume flux and water temperatures in May and June. A significant negative correlation between the Bering Strait ocean heat transport and Arctic sea ice extent in the Pacific sector is observed for May, June, and July, both within and outside the marginal ice zone, with a sharp decline in predictability for August and September.

Conclusion: The Bering Strait ocean heat transport is a skillful predictor for early melt season sea ice extent in the Pacific sector but loses predictive skills later in the summer in August and September due to changes in ice dynamics, in accordance with the loss of predictive skill in Global Climate Models.

Introduction

In recent decades, a sharp decline in sea ice extent (SIE), thickness, and age has been observed in the Arctic Ocean (1-3). These changes are projected to continue as per simulations using Coupled Model Intercomparison Project Phase 5 (CMIP5) under all representative concentration pathways (4). Increasing ocean heat is a significant contributor to sea ice decline (5). During the first large SIE decline of 2007, the heat transport through the Bering Strait was twice the 2001 heat flux, enough to account for approximately 30% of the estimated 2007 sea ice loss, and contributed to the creation of open water areas north of Bering Strait by May (6). Heat entering the broad shallow shelf of the Chukchi Sea (Fig. 1) interacts directly with the local sea-ice cover and can effectively reduce sea ice thickness before mixing with cooler waters from the central Arctic basin. Furthermore, dominant east-west sea ice drift in the winter and spring along the Alaskan coastline brings Pacific water heat from depth to the surface, due to coastal divergence and local Ekman offshore transport, leading to potentially thinner ice (7, 8). Additionally, loss of SIE and subsequent increases in the area of open water exposes ocean water to solar radiation directly, further warming the mixed layer and amplifying sea ice loss (i.e. the ice-albedo feedback) (9). While the volumetric transport through the Bering Strait is approximately 10% of the volume of the Fram Strait inflow, the yearly Bering Strait OHT (3 to 6×10^{20} Joules (J)) is the same order of magnitude as the Fram Strait OHT (5 to 13×10^{20} (J)) (5). The yearly OHT through the Barents Sea gate is significantly larger at approximately 2.21×10^{21} (J) (10). While outside the scope of this study, the transport of heat from the Atlantic Ocean via the Fram Strait and Barents Sea Gate plays a significant role in sea ice declines in the Atlantic Sector (11).

The Bering Strait, a narrow ~85-kilometer-wide channel between Alaska and Russia, is the only passage through which Pacific waters can enter the Arctic Ocean (5). The Bering Strait ocean heat transport (OHT) is a function of both water temperature and the volume transport of water through the strait. The large interannual variability of the Bering Strait OHT is thus the product of both the variability in the transport and temperature of the Bering Strait throughflow, which are themselves a function of both local and large-scale surface radiative and turbulent fluxes, surface winds, and internal oceanic variability (6). Quantifying the trends in Bering Strait OHT remains a difficult endeavor given the limited length of the Bering Strait throughflow observational record, and currently, increases in annual water transport through the strait are the sole observed independent trends (5).

Previous studies have sought to better understand the influence of the Bering Strait OHT on sea ice in the Chukchi Sea at seasonal timescales. Woodgate et al. (2010) hypothesize that the Bering Strait OHT acts to weaken ice, precipitating the onset of solar driven sea ice melt, and providing a wintertime subsurface heat source due to large residence times of Pacific waters in the Arctic Ocean (6). Serreze et al. (2016) investigate the predictability of sea ice retreat and advance dates in the Chukchi Sea using the Bering Strait OHT (12). They find that the April-June throughflow accounts for 68% of retreat day variance, and that July-September throughflow accounts for 67% of advanced date variance (12). Additionally, they find a strong significant correlation (r=0.8) between the Bering Sea OHT from 1990 to 2013 (excluding 1993 to 1996 due to data gaps) and sea ice retreat date (12). While Serreze et al (2016) report on the seasonal response between the Bering Strait OHT and Chukchi sea ice thermodynamics, questions regarding the monthly response of Chukchi SIE to Bering Strait OHT variability within the melt season has not yet been investigated.

This study analyzes the variability and predictability of the Bering Strait OHT to better understand the sensitivity of Arctic Ocean SIE to Pacific Ocean heat fluxes at monthly timescales. We first assess the interannual and monthly variability of the Bering Strait OHT and then calculate the monthly, regional covariance of SIE and the Bering Strait OHT in the Chukchi and East Siberian Seas (ESS). Thirdly, we assess the spatial variability of the response of SIE across the Arctic Ocean in the context of melt season reductions in monthly maximum sea ice extents, and the marginal ice zone, where SIE is seasonally variable. The applications of these findings to seasonal sea ice forecasting are also discussed.

Methods

Bering Strait Ocean Heat Transport

The Bering Strait OHT was calculated using monthly averages of hourly, corrected, near-bottom temperature and transport observations from 1997 to 2015 from the A3 mooring (see Fig. 1b below), collected by Wood-

†Editor Note: figures are adapted for print in black and white. View the coloured version online at msurj.com.

gate (2018) (5, 13). The dataset was post-processed in order to remove erroneous data and correct for sensor calibration errors (5). The A3 mooring is located approximately 35 kilometers north of the Bering Strait proper (Fig. 1b) and at a depth of 57 meters, roughly between 10 and 20 meters above the sea floor (5). This mooring was chosen based on the consistency and quality of the observational record and because its location in the outlet of the Bering Strait limits the influence of in-strait variations of velocity, temperature, or other parameters. Moorings A1 and A2, which are located in the Russian and US regions of the strait respectively, have temporally inconsistent and uncorrected records; and do not provide representative OHT estimates for the entire strait (5). Data from the A3 mooring, however, does not provide absolute OHT measurements due to its inability to account for the contribution of the Alaskan Coastal Current (ACC) (5). For the complete Bering Strait OHT, A3 recordings must be added to data from the A4 mooring, which was installed within the Strait off the Alaskan Coast in 2001 to better understand the role of the ACC in the Bering Strait throughflow (5). Due to the limited length of the A4 time series, it is not utilized in OHT calculations, resulting in the underestimation of the Bering Strait OHT. Nonetheless, the A3 mooring provides a sufficiently representative record to understand the relative variability of the throughflow and its influence on SIE in the Arctic Ocean (10). For more information of the mooring data used in this study, see Woodgate et al. (2018) and Woodgate (2015) (5, 13).

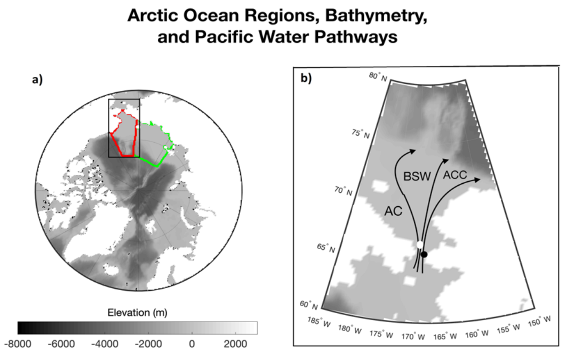

Figure 1. a) Bathymetry of Arctic Ocean and key regions. The Chukchi Sea is outlined in red and the East Siberian Sea is outline in green. Land areas are assigned a value of 3000 (m); b) pathways of Pacific waters (AC, Anadyr Current; BSW, Bering Shelf Water; and ACC, Alaskan Coastal Current) into the Chukchi Sea and Arctic Ocean. The approximate locations of the A3 (white) and A4 (black) moorings are shown. Plot (b) is adapted from Mathis et al. (2007) [19] (Note from the editor: figures are adapted for print in black and white. View the full coloured version online at msurj.com.)

The cumulative Bering Strait OHT, from Woodgate (2018), as assessed from January to month m, can be written as:

$$OHT_m = k\rho c_p \sum_{n=1}^{m} \left(T - T_{ref}\right)_n V_n P_n$$

Where ρ is the density of ocean water assumed to constant (1023 kg/m^3), c_p is the specific heat of ocean water (3900 J/kgK), T is the monthly mean observed near-bottom temperature of water, which is considered representative of water column, in the Bering Strait in month n, T_{ref} is the reference freezing point temperature (-1.9 °C) of ocean water at an approximate salinity of 32.5 psu. OHT is computed as relative to a reference freezing temperature at which Bering Strait waters leave the Arctic Ocean through the Fram Strait and Canadian Arctic Archipelago, thus allowing for the estimation of how much heat from Pacific waters has been lost to the Arctic Ocean throughout its transit (5). V_n (m^3/s) is the monthly mean volumetric transport of water through the Bering Strait during month n, P_n is the length of each month (s), and k (10^6) is a conversion factor (5). While the use of constant density, salinity, and reference temperature values introduces additional uncertainty to the OHT time series, Woodgate (2018) found that a salinity dependent reference freezing temperature would have relatively insignificant influence on the time series, only modifying OHT calculations by approximately 5% (5). Additionally, the use of a reference freezing point allows for a starting month of January, as wintertime months negligibly contribute to melt season OHT. The calculated Bering Strait OHT time series was detrended based on climatology before any statistical analyses were performed. For the purposes of examining the interannual variability of OHT, a monthly non-cumulative OHT time series was also created.

Sea Ice Extent

Arctic SIE is assessed using the *NOAA/NSIDC Climate Data Record of Passive Microwave Sea Ice Concentration* (14), dating back to November 1978. The dataset is based on brightness temperatures from the Special Sensor Microwave Imager/Sounder (SSMIS), the Special Sensor Microwave/Imager (SSM/I), and the Scanning Multichannel Microwave Radiometer (SMMR) to differentiate between sea ice and open water (14). Brightness temperatures are converted to sea ice concentration measurements using a rule-based classification (CDR algorithm) that relies on the highest output of two different proven algorithms, NASA Team and NASA Bootstrap (15). The dataset uses the Equal-Area Scalable Earth Grid (EASE-Grid), in which each grid cell has an area of 625 km^2 (15). We use the monthly resolution version of the NSIDC-CDR dataset.

SIE is defined as the sum of grid cells with greater than or equal to 15% sea ice coverage multiplied by the area of each grid cell. Grid cells with sea ice concentrations below 15% are considered to be open water. We define regions of the Chukchi and East Siberian Seas according to the NSIDC Arctic Ocean regional mask (see Fig. 1a above). Similar to OHT time series, SIE time series were detrended based on climatology before statistical analyses were conducted.

Results

Bering Strait Ocean Heat Transport Temporal Variability

Cumulative and non-cumulative heat transport through the Bering Strait was calculated from 1997 to 2015 (see Fig. 2-3). The non-cumulative OHT time series (see Fig. 3) shows that the use of a reference freezing temperature resulted in OHT values of 0 from January through April, which increase throughout the melt season from May to September, when the non-cumulative monthly transport is the largest, and then rapidly decreases during the fall. Interannual variability follows these seasonal cycles for both time series, increasing as the melt season progresses, with the least interannual variability throughout the melt season in May, and the most in September. As seen in Fig. 2, interannual variability has nearly doubled since 2010, with the range of observed cumulative September fluxes since 2010 at 2.31×10^{20} Joules (J) compared to 1.37×10^{20} J from 1997 – 2005. Additionally, the years 2007, 2011, 2015, which showed the largest September OHTs, were accompanied by anomalous OHT early in the summer (in May and June) unlike other years when the OHT anomalies starts in mid-summer in July. Percent change is used as an additional metric for Bering Strait OHT variability because of the magnitude scale differences between May and September heat fluxes. There is minimal variation in percent change throughout the year, with the exception of 2015, in which the May percent increase exceeded the September percent increase by ap-

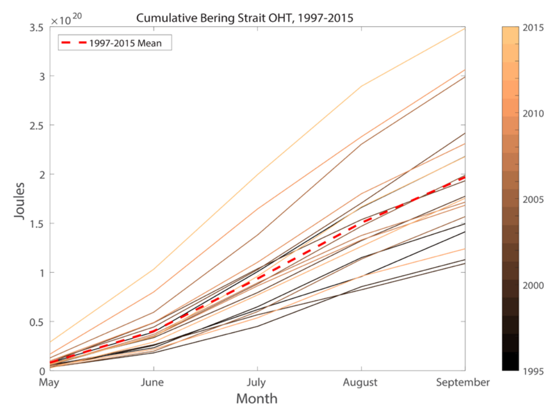

Figure 2. Cumulative monthly mean Bering Strait OHT (in Joules) from May of a given year through June-September of the same year. OHT values are relative to -1.9 ° C.

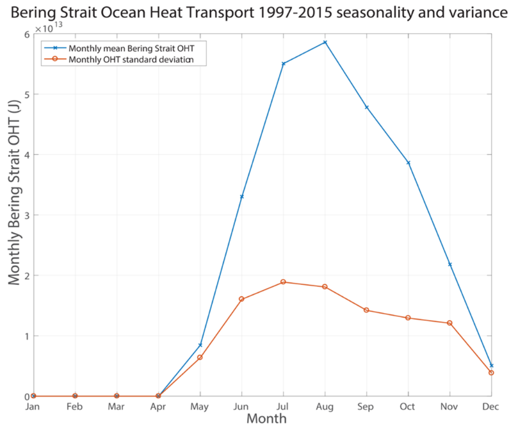

Figure 3. Monthly mean and standard deviation of Bering Strait OHT (in Joules) from 1997 to 2015. OHT values are relative to -1.9 °C.

Regional Predictability

Month to month correlations were calculated between the Bering Strait OHT and SIE in the Chukchi Sea (see Table 1). Correlation coefficients above r>|0.43| are statistically significant to the 95% confidence level using the standard t-test, and were found for the May, June, and July Bering Strait OHTs correlated with Chukchi SIEs over the same months. No significant correlations were found for August or September OHTs or SIEs. The largest significant correlations are seen in July SIEs with June and July Bering Strait OHTs which are correlated at r≈-0.8, while the lowest significant correlation is observed between the May Bering Strait OHT and May Chukchi SIE at r=-0.478. Between May and July, the strength of the correlation increases as the melt season progresses. Month to month correlations were also calculated between the Bering Strait OHT and SIE in the East Siberian Sea (ESS) (see Table 1). Significant correlations are observed primarily in June SIE, with an insignificant positive correlation observed in May, and insignificant negative correlations in August and September. May OHTs were significantly correlated with July SIEs at exactly r=0.44, while June and July OHTs were correlated with July SIEs at slightly below the 95% significance threshold.

Chukchi Sea	May SIE	June SIE	July SIE	August SIE	September SIE
May OHT	**-0.48**	**-0.63**	**-0.71**	-0.30	-0.17
June OHT	-	**-0.70**	**-0.8**	-0.35	-0.21
July OHT	-	-	**-0.82**	-0.36	-0.23
August OHT	-	-	-	-0.35	-0.25
September OHT	-	-	-	-	-0.24
ESS	May SIE	June SIE	July SIE	August SIE	September SIE
May OHT	0.23	**-0.63**	**-0.44**	-0.16	-0.08
June OHT	-	**-0.70**	-0.43	-0.17	-0.1
July OHT	-	-	-0.43	-0.20	-0.13
August OHT	-	-	-	-0.25	-0.19
September OHT	-	-	-	-	-0.17

Table 1. Correlation matrices between monthly Bering Strait OHT anomaly for month x and monthly mean Chukchi Sea and East Siberian Sea (ESS) SIE anomaly for month y. Correlations are 95% significant when |r|>0.43. Significant correlations are shown in bold.

The sharp decline in late summer predictability is also seen in the anomaly persistence of the Bering Strait OHT and Chukchi SIE. Anomaly persistence describes the influence of the variability of a climatologically detrended parameter later in its time series, and is calculated by correlating a given initial month with subsequent months of the same variable. Fig. 4 describes the anomaly persistence of the Bering Strait OHT and Chukchi SIE throughout the melt season. Bering Strait OHT anomalies have large significant persistence throughout the melt season from May through September with all intermonth correlations larger than 0.85. The persistence of Chukchi Sea SIE initialized in May shows a sharp continuous decline throughout the melt season, with significant persistence from May until July and insignificant persistence in August and September. Chukchi Sea SIE persistence for June and July shows a similar pattern, with a significant relationship for the first subsequent month, but then insignificant persistence in later months. Additionally, August Chukchi Sea SIE has high significant persistence with September SIE, with a correlation of r=0.83 (not shown).

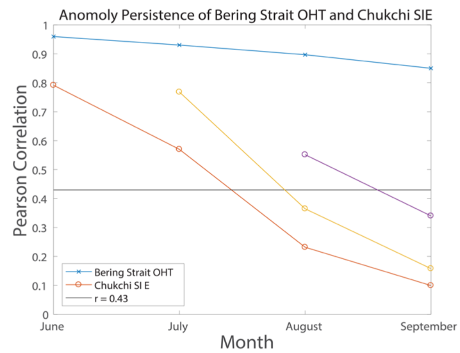

Figure 4. Anomaly persistence of the Bering Strait OHT (blue) and Chukchi SIE, from May to June through May to September (red), June to July through June to September (yellow), and July to August and September (purple). Correlations are 95% significant when r >0.43 (black).

Spatial Correlations

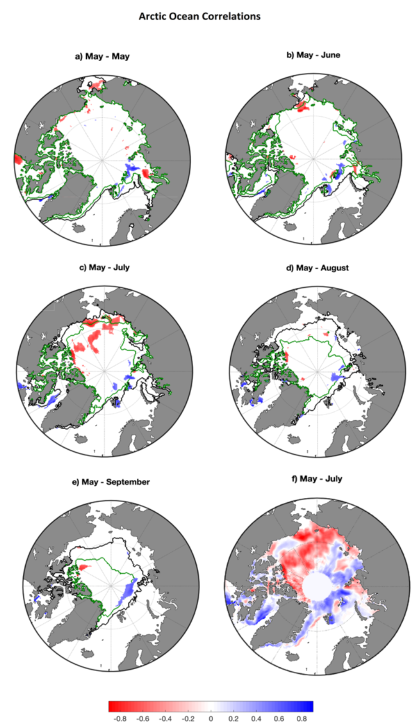

Figure 5. Significant Pearson correlations (≥95%) across the Arctic Ocean for a) May Bering Strait OHT and May SIE, b) May Bering Strait OHT June SIE, c) May Bering Strait OHT and July SIE, d) May Bering Strait OHT and August SIE, and e) May Bering Strait OHT and September SIE; f) shows all correlations between May Bering Strait OHT and July SIE. For a-e), the median maximum monthly SIE is outlined in black, and the minimum maximum monthly SIE is outlined in green.

Correlations between the Bering Strait OHT with the SIE were performed on a grid-cell basis in the Arctic Ocean (see Fig. 5). For May-May, May-June, and May-July correlations (Fig 5a-c), regions of the Arctic Ocean with the highest correlations are in close proximity to the median ice edge. This means that in May, the region with the largest extent of significant negative correlations lies south of the Bering Strait; in June, the largest negative correlations are seen north of the mouth of the strait; and in July, further into the interior of the Chukchi Sea. Additionally, in July, there is an enlargement of the affected region in the Arctic Ocean to include regions of the ESS and the northern and eastern Beaufort Gyre. In Fig. 5d and 5e, the correlation maps of the May Bering Strait OHT and August and September SIE respectively, show an extreme reduction in regions affected by the Bering Strait OHT. For all months shown, affected regions include those both within and outside the marginal ice zone.

Positive correlations are observed in the Atlantic sector of the Arctic Ocean in areas near the median ice edge. For the May-May correlations (Fig. 5a), a positive signal is observed in the northern regions of the Barents and Kara Seas. For the May-June correlations (Fig. 5b), the signal is observed in the same regions but with a larger spatial extent. In the Barents and Kara Seas, the May-July (Fig. 5c) correlation shows a similar affected region to the May-May correlations, with the addition of significant positive correlations in the Baffin and Hudson Bays. Both the western and eastern regions of the Arctic Ocean see significant correlations with larger spatial extents when correlations are lagged, as seen in Fig. 5c. Additionally, a subseasonal oscillation is observed in the Hudson Bay, whereby, in May and June, a significant negative correlation is seen in the Western Hudson Bay, only to diminish in July and be replaced by significant positive correlations in Eastern Hudson Bay, which do not appear in May or June.

Discussion

May Bering Strait OHT is a skillful predictor for anomalously large September ocean heat fluxes, as seen in the large anomaly persistence throughout the entirety of the melt season in Fig. 5, and the large May and September OHTs in 2007, 2011, and 2015, as seen in Fig. 2-3. Woodgate (2018) finds that the anomalously large OHTs of 2007, 2011, and 2015 are due to the early arrival of warm waters by approximately 20 days, as well as rapid spring atmospheric warming (5). Increasing spring rapid warming leading to early sea ice breakup south of, and within, the Bering Strait, partially explains the increased OHT, and its associated variability. Sea ice breakup exposes ocean water to surface winds, increasing water velocity, which can increase transport into the Arctic, and thus increase variability.

The Bering Strait OHT has the greatest influence on Arctic SIE near the median monthly ice edge, which is expected given that the edges of the ice pack are most vulnerable to melt, especially from oceanic heat entering the Arctic Ocean from the south. This northward shift of the influence of the Bering Strait OHT throughout the melt season from the southern Bering Strait into the Chukchi Sea, and then further north into the western Arctic Ocean explains the increasing predictability trend from May through July. For May, the median monthly maximum SIE extends beyond the Bering Strait, thus a significant portion of the significant correlation is not included within the geographic limits of the Chukchi Sea. This is in contrast to June and July SIEs, in which the median maximum ice extent intersects the bounds of the Chukchi Sea, centering the OHT-effected regions within the Chukchi Sea limits, and thus producing a larger regional correlation. For August and September SIEs, the median ice edge is within the limits of the Chukchi Sea, but the region with significant correlations is reduced compared to earlier months, suggesting that the late summer decline in predictability is due to changes in sea ice dynamic and thermodynamic processes, such as drift (wind) and the ice-albedo feedback. Additionally, due to presence of significant correlations outside the marginal ice zone and within the minimum ice edges, we can conclude that the decline of predictability is due to dynamics and not due to the regions becoming ice-free. We hypothesize that significant positive correlations in the Atlantic sector of the Arctic Ocean are caused by increases in the volume flux through the Bering Strait leading to decreased OHT through the Fram Strait and Barents Sea Gate, and thus increased SIE, due to the conservation of water mass of the Arctic Ocean, as seen in Jahn et al. (2010) (16). These conclusions are also supported by Auclair & Tremblay (2018), who utilized the Community Earth System Model Large Ensemble (CESM-LE) to test the relationship between different OHTs and rapid sea ice declines, in which absorbed shortwave radiation by the ocean from May through September was significantly, negatively correlated with Bering Strait OHT anomalies in the Barents and Kara Seas, also suggesting a positive relationship between the Bering Strait OHT and SIE in the Atlantic sector of the Arctic Ocean (11).

We find that May Bering Strait OHT is a poor predictor for the end of summer (August and September) SIE in the Chukchi Sea (see Table 1). These conclusions are also supported by Auclair & Tremblay (2018), who posit that OHTs had the greatest influence on SIE over shallow continental shelves, in which the majority of heat remains in the mixed layer, whereas in the Arctic basin, vertical heat transport is reliant on Ekman pumping, thus decreasing the exposure of retreated pack ice to oceanic heat (11). They also found decreased coverage of significant negative correlations between Bering Strait OHT anomalies and Chukchi SIE, in agreement with our findings (11). The diminished influence of Bering Strait OHT on late summer SIE is in accord with the idea of a predictability barrier for the summer SIE, as investigated in model-based forecast studies by Day et al. (2014) and Bushuk et al. (2017) (17, 18). Using perfect-model experiments based on the Geophysical Fluid Dynamics Laboratory seasonal prediction system, Bushuk et al. found that predictions of September SIE in the Chukchi Sea are skillful up to a lead time of two months – i.e.: there is a sharp loss of skill for forecasts initialized before July, hence a 'July barrier for predictability' (18). Our findings of a lack of correlation between early summer OHT and late summer SIE support the idea that late summer thermodynamic and dynamic processes, such as surface winds, air temperatures, and open water exposed to direct solar heating, drive the variability of summer SIE in the Chukchi Sea, overriding any early-season signature from ocean heat (9). Our results and hypothesized mechanisms, however, also suggest a significant role that the Bering Strait OHT plays on early-summer SIE (up to July), in agreement with Serreze et al. (2016), who note that the April to June oceanic heat inflow through the Bering Strait is strongly correlated with the retreat date of sea ice in the Chukchi Sea (12). Anomalies in other parameters such as sea ice thickness may have longer memory, enabling skillful September sea ice predictions from as early as May (18). Additionally, our findings illustrate the inherent complexity of predicting SIE via global climate models, in which a multitude of parameters gain and lose predictive ability throughout the year.

More work is required in order to adequately explain several of the results of this study. Firstly, there is a discrepancy between the ESS regional correlations and the July spatial correlations, outlined in Table 1 and Fig. 5 respectively. The spatial extent of the negative signal in the ESS in Fig. 5c, would suggest significant regional correlations in July in addition to June. This discrepancy is the result of insignificant positive correlations in other regions of the ESS as seen in Fig. 5f, which partially oppose the negative correlations enough to bring the regional signal to below the 95% significance level. More work, however, is required in order to understand the source of this positive signal in the ESS in July. Secondly, Serreze et al (2016), found a significant correlation (~0.67) between July through September Bering Strait OHT and sea ice advance date in the Chukchi Sea, whereas we found no significant correlations between the May through September Bering Strait OHT and September sea ice extent (12). This predictability disparity is unexpected given the similarity between advanced date, first date of the year when sea ice concentration exceeds 30%, and SIE, as well as the agreement between early melt season retreat date and SIE predictabilities (12). Additionally, the high persistence of Bering Strait OHT anomalies suggests that it is highly unlikely that the discrepancies in heat flux start date (July vs. May) are responsible for the large differences in predictability. This discrepancy is likely due to different regional definitions of the Chukchi Sea, which in Serreze et al (2016) is not defined beyond the broad-shallow shelf, whereas our boundaries extend into the deeper waters of the Arctic Ocean interior (12). More research on the differing mechanisms governing Chukchi Sea advanced date and SIE beyond the Chukchi Sea shelf is required in order to understand this disagreement.

Conclusion

This study investigated the relationship between the Bering Strait ocean heat transport (OHT) and sea ice extent (SIE) in the western Arctic Ocean at monthly time scales, as well as patterns in variability and predictability across the Bering Strait OHT time series from 1997 to 2015. We found increased variability in the Bering Strait OHT since 2010, with large heat flux anomalies early in the melt season in May and June as strong predictors for large September OHTs. Strong negative correlations were observed between Bering Strait OHT and SIE in the Chukchi Sea during May, June, and July, with a sharp decline in predictability for August and September. High predictability was also found between May Bering Strait OHT flux and July SIE in the Northern and Eastern Beaufort Gyre, as well as along the Siberian Coast and parts of the East Siberian Sea. These results not only contribute to our understanding of ice-ocean dynamics in the Arctic Ocean, but also provide observational evidence in support of SIE predictability for both seasonal forecasts and global climate models. Improved sea ice prediction will help ensure the safe functioning of industrial and shipping operations in the Arctic Ocean as the Arctic takes on greater global economic importance.

Acknowledgements

We would like to thank the McGill School of Environment and Department of Atmospheric and Oceanic Sciences for their support throughout this research, and our three anonymous reviewers for their constructive feedback.

References

1. Stroeve J, Holland MM, Meier W, Scambos T, Serreze M. Arctic sea ice decline: Faster than forecast. Geophysical Research Letters. 2007Jan;34(9).

2. Kwok R, Rothrock DA. Decline in Arctic sea ice thickness from submarine and ICESat records: 1958-2008. Geophysical Research Letters. 2009 Jun;36(15).

3. Maslanik JA, Fowler C, Stroeve J, Drobot S, Zwally J, Yi D, et al. A younger, thinner Arctic ice cover: Increased potential for rapid, extensive sea-ice loss. Geophysical Research Letters. 2007;34(24).

4. Stroeve J, Notz D. Changing state of Arctic sea ice across all seasons. Environmental Research Letters. 2018;13(10):103001.

5. Woodgate RA. Increases in the Pacific inflow to the Arctic from 1990 to 2015, and insights into seasonal trends and driving mechanisms from year-round Bering Strait mooring data. Progress in Oceanography. 2018;160:124–54.

6. Woodgate RA, Weingartner T, Lindsay R. The 2007 Bering Strait oceanic heat flux and anomalous Arctic sea-ice retreat. Geophysical Research Letters. 2010;37(1).

7. Holland MM, Bitz CM, Tremblay B. Future abrupt reductions in the summer Arctic sea ice. Geophysical Research Letters. 2006 Dec;33(23).

8. Pickart RS, Moore G, Mao C, Bahr F, Nobre C, Weingartner TJ. Circulation of winter water on the Chukchi shelf in early Summer. Deep Sea Research Part II: Topical Studies in Oceanography. 2016;130:56–75.

9. Perovich DK, Light B, Eicken H, Jones KF, Runciman K, Nghiem SV. Increasing solar heating of the Arctic Ocean and adjacent seas, 1979–2005: Attribution and role in the ice-albedo feedback. Geophysical Research Letters. 2007 Nov;34(19).

10. Smedsrud LH, Esau I, Ingvaldsen RB, Eldevik T, Haugan PM, Li C, et al. The Role of The Barents Sea In The Arctic Climate System. Reviews of Geophysics. 2013;51(3):415–49.

11. Auclair G, Tremblay LB. The Role of Ocean Heat Transport in Rapid Sea Ice Declines in the Community Earth System Model Large Ensemble. Journal of Geophysical Research: Oceans. 2018 Nov;123: 8941-8957

12. Serreze MC, Crawford AD, Stroeve JC, Barrett AP, Woodgate RA. Variability, trends, and predictability of seasonal sea ice retreat and advance in the Chukchi Sea. Journal of Geophysical Research: Oceans. 2016;121(10):7308–25.

13. Woodgate R, Stafford K, Prahl F. A Synthesis of Year-Round Interdisciplinary Mooring Measurements in the Bering Strait (1990–2014) and the RUSALCA Years (2004–2011). Oceanography. 2015Jan;28(3):46–67. Available from: http://psc.apl.washington.edu/HLD/Bstrait/Data/BeringStraitCruiseDataArchive.html

14. Meier W, Fetterer F, Savoie M, Mallory S, Duerr R, et al. NOAA/NSIDC Climate Data Record of Passive Microwave Sea Ice Concentration, Version 3. 2017; NSIDC: National Snow and Ice Data Center.

15. Peng G, Meier WN, Scott DJ, Savoie MH. A long-term and reproducible passive microwave sea ice concentration data record for climate studies and monitoring. Earth System Science Data Discussions. 2013Jul;6(1):95–117.

16. Jahn A, Tremblay B, Mysak LA, Newton R. Effect of the large-scale atmospheric circulation on the variability of the Arctic Ocean freshwater export. Climate Dynamics. 2009;34(2-3):201–22.

17. Day JJ, Tietsche S, Hawkins E. Pan-Arctic and Regional Sea Ice Predictability: Initialization Month Dependence. Journal of Climate. 2014;27(12):4371–90.

18. Bushuk M, Msadek R, Winton M, Vecchi GA, Gudgel R, Rosati A, et al. Skillful regional prediction of Arctic sea ice on seasonal timescales. Geophysical Research Letters. 2017;44(10):4953–64.

19. Mathis JT, Pickart RS, Hansell DA, Kadko D, Bates NR. Eddy transport of organic carbon and nutrients from the Chukchi Shelf: Impact on the upper halocline of the western Arctic Ocean. Journal of Geophysical Research. 2007 Apr;112(C5).